CDDpress

www.nature.com/cdd

ARTICLE

Check for updates

SNORD88C guided 2′-O-methylation of *28S rRNA* regulates SCD1 translation to inhibit autophagy and promote growth and metastasis in non-small cell lung cancer

Kangyu Wang[1], Shiwen Wang[1], Yue Zhang[1], Li Xie[1], Xingguo Song[1]✉ and Xianrang Song[1,2]✉

Small nucleolar RNAs (snoRNAs) have been shown to play critical regulatory roles in cancer development. *SNORD88C*, which located at the intronic region of *C19orf48* in chromosome 19q.33 with a 97-nt length was screened through database and snoRNA-sequencing. We firstly verified this snoRNA was up-regulated in tissue and plasma and served as a non-invasive diagnostic biomarker; then confirmed that *SNORD88C* promoted proliferation and metastasis of NSCLC in vitro and in vivo. Mechanistically, *SNORD88C* promoted 2′-O-methylation modification at the C3680 site on *28S rRNA* and in turn enhanced downstream SCD1 translation, a central lipogenic enzyme for the synthesis of MUFA that can inhibit autophagy by regulating lipid peroxidation and mTOR, providing the novel insight into the regulation of *SNORD88C* in NSCLC.

Cell Death & Differentiation (2023) 30:341–355; https://doi.org/10.1038/s41418-022-01087-9

INTRODUCTION

Non-small cell lung cancer (NSCLC), which accounts for approximately 85% of lung cancer cases worldwide, is a highly malignant tumor and a leading cause of global cancer-related deaths [1]. Despite of continuous advances in the improvement of cancer treatment, only 16% of patients suffering from NSCLC survive within 5 years after diagnosis [2], because at that time approximately two-thirds of patients have presented with metastatic tumors [1]. Therefore, there is an urgent need to deepen our understanding of the mechanism of NSCLC progression and identify effective diagnostic biomarkers and new therapeutic targets.

Small nucleolar RNAs (snoRNAs), mid-size-long noncoding RNAs (ncRNAs), mainly locate within introns of protein-coding genes and long non-coding RNAs [3], and are divided into two categories according their structural basis: H/ACA snoRNAs (SNORAs) and Box C/D snoRNAs (SNORDs), SNORAs form complexes with dyskerin and are responsible for pseudouridynlation of rRNAs whereas SNORDs form the small nucleolar RNA-protein complexes (snoRNPs) with Fibrillarin (FBL) and guide 2′-O-methylation (2′-O-me) of rRNAs [4]. rRNA modification by snoRNAs, especially the 2′-O-me, impacts ribosome biogenesis [5], activity and fidelity of translation [6], then contributes to the regulation of tumorigenesis and progression [7]. For example, *SNORD12C/78* guided the 2′-O-me of *28SrRNA* at sites G3878 and G4593, then enhanced the translation activity of cancer-related proteins and in turn the malignant phenotype of colorectal cancer [8]. On the contrary, *SNORA23* impaired the methylation of G4593 on *28SrRNA* and inhibited the progression of hepatocellular carcinoma [9].

Accumulating studies have shown that snoRNAs are abnormally expressed in tumors and play an important role in tumor proliferation and metastasis through a variety of pathways. For example, *SNORA42A* was highly expressed in colorectal cancer, and promoted cell invasion and metastasis in vivo and in vitro [10]; *SNORD12B* in esophageal squamous cell carcinoma acted as an oncogene to promote tumor migration and invasion through AKT-mTOR-4EBP1 [11]. Notably, snoRNAs are stably expressed and measurable in body fluids including the blood plasma, serum, and urine of cancer patients, empowering them with the potential as the non-invasive biomarkers for diagnostics of malignancies. For example, plasma *SNORD33*, *SNORD66* and *SNORD76* acted as biomarkers for diagnosing lung cancer [12], whereas a six-snoRNAs panel possessed the favorable diagnostic efficiency for renal clear cell carcinoma (RCC) [13]. Our previous studies also demonstrated that *SNORD63* and *SNORD96A* were not only stable in plasma and urinary sediment, but also acted as reliable and promising diagnostic markers for RCC [14].

In this study, we used the database and sequencing results to screen a new oncogene. *SNORD88C* is located at the intronic region of *C19orf48* - the host gene of *SNORD88C* which is a long non-coding RNA (lncRNA) in chromosome 19q.33 with a 97-nt length. We firstly verified this snoRNA was up-regulated in tissue and plasma and served as a non-invasive diagnostic biomarker; then confirmed that *SNORD88C* promoted proliferation and metastasis of NSCLC in vitro and in vivo. Importantly, our data supported SCD1 was the direct downstream of *SNORD88C*. *SNORD88C* enhanced its translation activity though guiding 2′-O-me of *28S rRNA*, in turn inhibited autophagy to promote the

[1]Department of Clinical Laboratory, Shandong Cancer Hospital and Institute, Shandong First Medical University and Shandong Academy of Medical Sciences, Jinan, Shandong, China. [2]Shandong Provincial Key Laboratory of Radiation Oncology, Shandong Cancer Hospital and Institute, Shandong First Medical University and Shandong Academy of Medical Sciences, Jinan, Shandong, China. ✉email: xgsong@sdfmu.edu.cn; xrsong@sdfmu.edu.cn

Edited by E. Baehrecke

Received: 14 April 2022 Revised: 31 October 2022 Accepted: 1 November 2022
Published online: 14 November 2022

migration and invasion of NSCLC cells, providing the novel insight into the regulation of *SNORD88C* in NSCLC.

RESULTS

SNORD88C is up-regulated in NSCLC and serves as a non-invasive diagnostic biomarker

To identify snoRNAs aberrantly expressed in NSCLC, we analyzed the differential expressions of snoRNAs between tumor tissues (including lung adenocarcinoma (LUAD) and lung squamous carcinoma (LUSC)) and para-tumoral tissues in SNORic database from TCGA, the top 50 genes with the most significant difference were represented by heat map (Fig. S1A, B). Next, plasma from 4 healthy donors and 6 NSCLC patients were subjected to snoRNA sequencing, the volcano map demonstrated the differential snoRNAs (Fig. S1C), among which 12 up-regulated and 4 down-regulated snoRNAs were selected due to $P < 0.05$ (Fig. 1A). Finally, the differential snoRNAs mentioned above were subjected to VENN diagram analysis (Fig. 1B), and only *SNORD88C* was overlapped and chosen as the candidate.

We further verify the upregulation of *SNORD88C* in NSCLC. As shown in Fig. 1C, *SNORD88C* was significantly elevated in the tumor tissues compared to the para-tumor tissues in both TCGA data (left, 989 vs 91) and FFPE detection (right, 48 NSCLC and paired para-tumor tissues). We also analyzed the relationship between *SNORD88C* and clinicopathological parameters, which was related to the histopathologic type, T stage, and N stage (Fig. 2SA–C, Tables S1 and 1). Moreover, as shown in Fig. 1D up-regulated *SNORD88C* expression was also observed in early-stage NSCLC (I + II) compared with the normal tissue in both TCGA data (left, I + II = 784 vs 91) and FFPE detection (right, I + II = 34 pairs), implying its role in the the occurrence and development of NSCLC.

Further verification of *SNORD88C* level in the plasma from 178 healthy donors and 224 NSCLC patients (including I + II = 87) revealed its upregulation in NSCLC and early-stage NSCLC, consistently (Fig. 1E), which was significantly correlated with tumor size, and tumor progression, TNM stages (Fig. 2SD–I, Table 2). Notably, *SNORD88C* predominately expressed in vesicle-depleted plasma other than in exosomes and MVs (Fig. S2J) and was stable in the plasma as evidence from no obvious change observed after RNase A treatment or storage for 30 days (Fig. 1F). Meanwhile, ROC curves analysis was performed to investigate diagnosis efficacy, possessing the area under curve (AUC) for NSCLC and early-stage NSCLC was 0.7097 and 0.6406, respectively (Fig. 1G). Carcinoembryonic antigen (CEA), a traditional biomarker generally accepted clinically, possesses the poor clinic diagnostic efficiency for early-NSCLC. Nevertheless, the AUC of CEA for early-NSCLC was significantly elevated from 0.6650 to 0.7279 when combined with *SNORD88C* (Fig. 1H and Fig. S2K). Taken together, *SNORD88C* is up-regulated in NSCLC and serves as a non-invasive diagnostic biomarker.

SNORD88C promotes proliferation of NSCLC in vitro and in vivo

To elucidate the role of *SNORD88C in* NSCLC progression, we overexpressed or downregulated *SNORD88C* in three NSCLC cell lines (A549, H1299, and SPC-A1) according to their background expression (Fig. S3A). we also verified the transfection efficiency by q-PCR (Fig. S3B–F), as well as the effect of *SNORD88C* silencing on its host gene *C19orf48* (Fig. S3G–L), neither transient nor steady silencing of *SNORD88C* affected the expression of *C19orf48*. Next, CCK-8 and colony formation analysis were employed to determine the effect of *SNORD88C* on cell proliferation. As shown in Fig. 2A, *SNORD88C* knockdown significantly suppressed cell viability of A549 and H1299 cells; On the contrary, forced *SNORD88C* expression enhanced growth in SPC-A1 and H1299 cells (Fig. 2B). Consistently, A549 and H1299 cells with silencing *SNORD88C* showed suspended clonogenicity, whereas *SNORD88C* overexpression caused obvious increase in the colony-formation ability of SPC-A1 and H1299 cells (Fig. 2C, D).

To determine the effects of *SNORD88C* on NSCLC proliferation in vivo, we established xenograft nude mouse model using A549 cells with *SNORD88C* stable knockdown (LV-sh-*SNORD88C*) or not (LV-sh-NC) (Fig. S3F). As expected, xenografts in LV-sh-*SNORD88C* group grew significantly slower than those in control group (Fig. 2E) and showed a significant decrease in tumor weight and volume compared to the control (Fig. 2F, G). Immunohistochemistry staining for Caspase-3 and Ki67 revealed that LV-sh-*SNORD88C* promoted apoptosis but inhibited proliferation in A549 xenografts (Fig. 2H). In summary, *SNORD88C* acts as a regulator of proliferation in NSCLC in vitro and in vivo.

SNORD88C promotes NSCLC migration and invasion in vitro and in vivo

As described above, the elevated *SNORD88C* was related with tumor progression in the TCGA database and plasma detection, thus, we next determined its role in migration and invasion. The wound healing assays revealed that the mobility was dramatically inhibited by *SNORD88C* knockdown in A549 and H1299 cells, but promoted by its overexpression in H1299 and SPC-A1 cells (Fig. 3A and S4A). Moreover, A549 and H1299 cells displayed significantly decreased migration and invasion abilities after silencing *SNORD88C* expression, but these abilities were stimulated remarkably by overexpressed *SNORD88C* (Figs. 3B and S4B). Considering the crucial role of EMT in invasion and migration, we then detected effect of *SNORD88C* on EMT-related protein expression. As shown in Fig. 3C, *SNORD88C* knockdown increased E-cadherin but suppressed N-cadherin, Vimentin, and Snail in A549 and H1299 cells, whereas *SNORD88C* overexpression displayed the opposite effect in SPC-A1 and H1299 cells.

Furthermore, we established the pulmonary metastasis model by injecting A549 cells with stably *SNORD88C* knockdown and firefly luciferase expression to the tail vein of the nude mice. As expected, in vivo bioluminescence imaging (BLI) showed the luciferase signal intensities in the LV-sh-*SNORD88C* group was remarkably lower than that in the control (Fig. 3D). After lung tissues separation, fewer metastatic loci occurred in the murine lungs in the LV-sh-*SNORD88C* group than those in the control group (Fig. 3E). Besides, H&E staining demonstrated some metastatic loci invaded the lung capsule in the LV-sh-NC group but none was observed in the LV-sh-*SNORD88C* group (Fig. 3F). These results demonstrate that *SNORD88C* promotes NSCLC migration and invasion in vitro and in vivo.

SNORD88C-attenuated autophagy is required for its promotion of migration and invasion

To explore the downstream target genes of *SNORD88C*, LC-MS/MS-based TMT-labeled quantitative proteomic was employed in the H1299 with silencing *SNORD88C* or negative control. As shown in Fig. 4A, a total of 384 up-regulated proteins and 369 down-regulated proteins were presented at the volcano map due to *p*-value ≤ 0.05 and FC ≥ 1.2, most of which were enriched in metabolism related pathways (Fig. 4B).

Autophagy, as it is routinely referred to, allows cells to maintain metabolic sufficiency and survive under conditions of nutrient stress and can be regulated by multiple metabolic pathways. Hence, we further detected the effect of *SNORD88C* on autophagy. As shown in Fig. 4C, autophagy was activated by *SNORD88C* knockdown both in A549 and H1299 cells whereas *SNORD88C* overexpression displayed the inhibitory effect on autophagy in SPC-A1 and H1299 cells. Accordingly, *SNORD88C*-attenuated autophagy was also verified by immunofluorescence labeled by anti-LC3 antibody to show the formation of autophagosomes, which demonstrated an increase in the number of autophagosomes by *SNORD88C* knockdown but a decrease by *SNORD88C* overexpression (Figs. 4D, S5A, B). Next, this phenomenon was

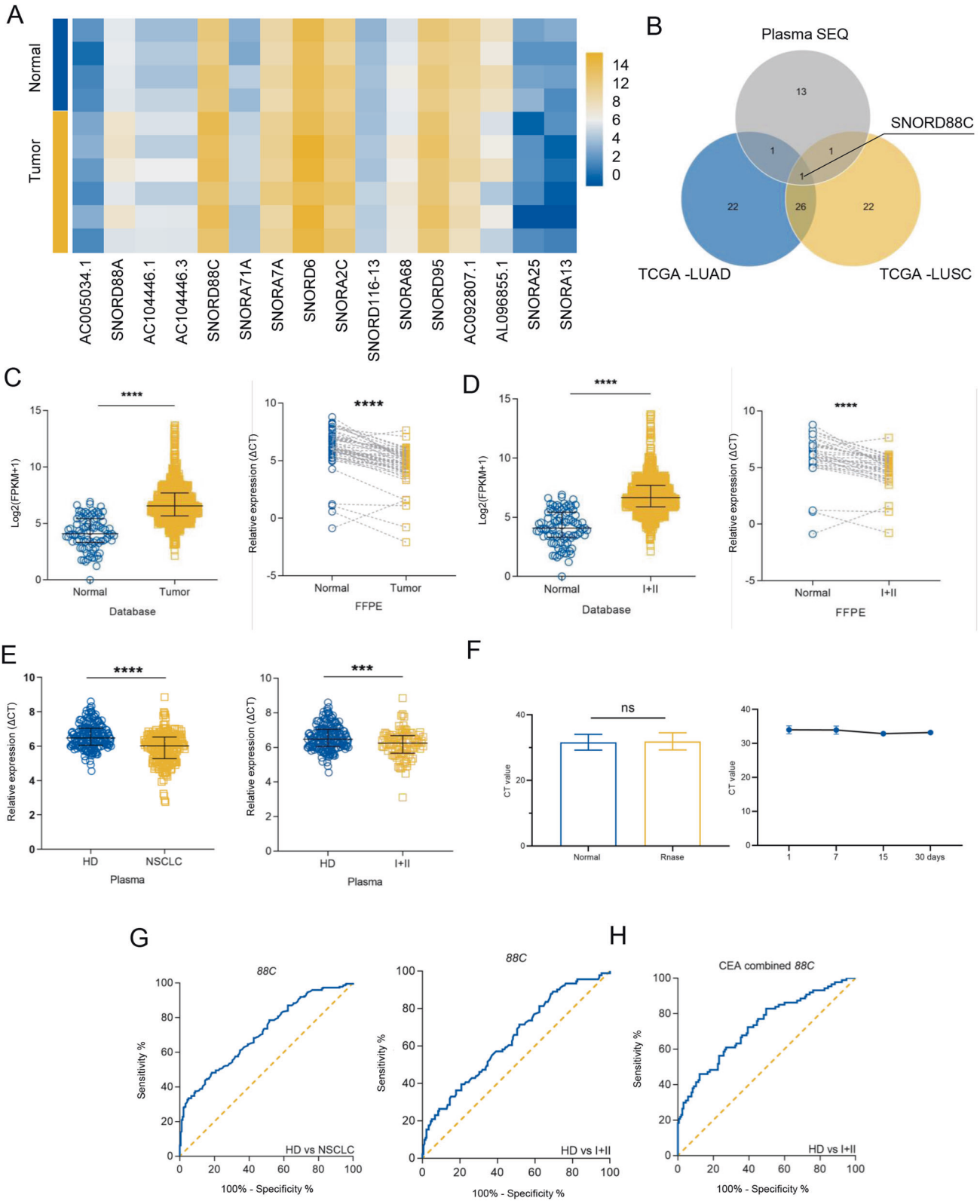

further confirmed by transmission electron microscope (TEM). Ultrastructurally, *SNORD88C* knockdown significantly increased whereas *SNORD88C* overexpression decreased the autophagy vacuoles in numbers as shown in Figs. 4E, S5C, D. Furthermore, we confirmed the role of *SNORD88C* in autophagy flux via transfection of adenovirus-mediated mRFP-GFP-LC3 vector, which labelled autophagosomes yellow because of superposition of GFP and mRFP signals, and autolysosomes red as the low lysosomal pH quenches the GFP signal [15]. As shown in Figs. 4F, S5E, most of the puncta lost the GFP signal and retained the mRFP signal in *SNORD88C* silencing or overexpressed cells like that in the rapamycin-treated cells, but unlike that in cells treated by Baf-

Fig. 1 *SNORD88C* is up-regulated in NSCLC and serves as a non-invasive diagnostic biomarker. A Though the snoRNAs-sequencing in plasma from NSCLC patients and donors, the differential snoRNAs was shown by heatmap. **B** The top 50 snoRNAs with the largest fold change in the LUAD and LUSC data sets from TCGA and the statistically differential snoRNAs in the sequencing results were analyzed using the VENN diagram, in which only *SNORD88C* was overlapped. **C**, **D** *SNORD88C* was significantly increased in NSCLC and early NSCLC tissues from TCGA database and FFPE samples, compared with para-tumor tissues (**E**) *SNORD88C* was significantly increased in the plasma of NSCLC and early NSCLC patients, compared with the plasma of donors. **F** *SNORD88C* was stably expressed in plasma treated with RNase (left) or stored at −80 °C at time-points of 1, 7, 15, 30 days (right). **G** The diagnostic efficacy of plasma *SNORD88C* for NSCLC (left) and early-NSCLC (right). **H** The diagnostic efficacy of *SNORD88C* combined with CEA for early-NSCLC. Two-tailed paired *t*-test, two-tailed unpaired *t*-test, Mann-Whitney test, one-way analysis of variance (ANOVA) or Kruskal-Wallis test; ns, no significance; $^{*}P < 0.05$, $^{**}P < 0.01$, $^{***}P < 0.001$, $^{****}P < 0.0001$.

A1, quenching of the GFP was significantly diminished, indicating that *SNORD88C* demonstrated little impact on autophagy flux. Next, we investigated whether the mTOR/ULK1 signaling contributes to *SNORD88C*-attenuated autophagy. As shown in Fig. 4G, *SNORD88C* knockdown led to downregulation of phosphorylations of MTOR and its downstream proteins P70S6K and ULK1 in A549, while phosphorylations of these proteins were increased after *SNORD88C* overexpression in H1299. Notably, AMPK phosphorylation was not affected by *SNORD88C*, indicating *SNORD88C* regulated mTOR/ULK1 signaling independent on AMPK (Fig. 4G).

To provide a direct link between *SNORD88C*-attenuated autophagy and it-induced migration and invasion of lung cancer cells, NSCLC cells were transfected with *ATG5* siRNA (si-*ATG5*) and plasmid (p-*ATG5*) (Figs. 4H, S5F), as well as treated with 3-Methyladenine (3-MA) or rapamycin (Fig. S5G, H) followed by migration and invasion detection. *si-ATG5* and 3-MA could abolish the suppressive effect on migration and invasion caused by *SNORD88C* silencing in A549 cells, whereas the metastatic effect of H1299 enhanced by *SNORD88C* overexpression was reversed at least partially by p-*ATG5* or rapamycin addition. Overall, these results support that *SNORD88C* suppresses autophagy and then promote the migration and invasion of NSCLC cells.

SNORD88C inhibits autophagy via upregulating SCD1 protein expression

To figure out the metabolites involved in *SNORD88C*-attenuated autophagy, GC-MS-based metabolomics targeting fatty acids were performed in H1299 cells with *SNORD88C* knockdown since pathway of unsaturated fatty acids biosynthesis was enriched in above LC-MS/MS-based TMT-labeled quantitative proteomic (Fig. 4B). As shown in Figs. 5A, S6A, many kinds of unsaturated fatty acids were decreased in *SNORD88C* knockdown cells compared to the control, among which the decease of oleic acid (OA), a monounsaturated fatty acid (MUFA), seemed more significant, indicating *SNORD88C* played a crucial role in lipid accumulation and peroxidation. Hence, C11-bodipy staining was employed, and flow cytometry analysis showed that lipid peroxidation was promoted by silencing *SNORD88C* but inhibited by its overexpression (Figs. 5B, S6C), consistent with the result that *SNORD88C* could inhibit autophagy.

Stearoyl-CoA desaturase 1 (SCD1) is a central lipogenic enzyme for the synthesis of MUFA, which also exhibited the most significant change in above LC-MS/MS-based TMT-labeled quantitative proteomic (Fig. S6B) after silencing *SNORD88C*. Importantly, western blot assays successfully validated *SNORD88C* positively regulated SCD1 protein level, which was decreased by *SNORD88C* knockdown in A549 and H1299 cells but increased significantly after *SNORD88C* overexpression in H1299 and SPC-A1 cells (Figs. 5C, S6D). Accordingly, flow cytometry analysis showed that the promotion of silencing *SNORD88C*, as well as the inhibitory effect of *SNORD88C* overexpression on lipid peroxidation could be successfully reversed by *SCD1* overexpression and knockdown, respectively (Figs. 5D, S6E), suggesting *SNORD88C* inhibited lipid peroxidation via upregulating SCD1 protein expression.

Furthermore, we explored the role of SCD1 in *SNORD88C*-attenuated autophagy. As shown in Figs . 5E, S6F, overexpression of *SCD1* could restore autophagy activation by *SNORD88C* knockdown in A549 cells, as evidence from the decrease in LC3B expression in the *SNORD88C*-knockdown plus *SCD1*-overexpression group; Consistently, *SCD1* silencing relieved autophagy inhibition by *SNORD88C* overexpression. Besides, we also observed the effects of *SNORD88C* and *SCD1* on mTOR pathway. As expected, SCD1 abolished the effect of *SNORD88C* on mTOR pathway related protein, including *p*MTOR, *p*P70S6K, *p*ULK1 (Fig. 5F), indicating *SNORD88C* might promote SCD1 protein expression, then accelerate MUFA synthesis, inhibit lipid peroxidation, affect mTOR pathway and finally inhibit autophagy.

Finally, we examined the direct link between *SNORD88C*/SCD1 axis and migration and invasion of lung cancer cells. As shown in Figs. 5G, H, S6G-J, *SCD1* overexpression reversed the inhibitory effect on migration and invasion in A549 and H1299 cells after *SNORD88C* silencing, while *SCD1* knockdown abolished the promotion *of SNORD88C* overexpression on lung cancer cell metastasis in SPC-A1 and H1299 cells. Likewise, SCD1 abolished the effect of *SNORD88C* on EMT pathway-related protein, including N-cadherin, Vimentin, and E-cadherin (Fig. S6K). Taken together, these results suggest that SCD1 was the downstream regulatory protein of *SNORD88C* and promoted the migration and invasion of NSCLC cells by inhibiting autophagy.

SNORD88C regulates the translation activity of SCD1 though guiding 2′-O-me of *28S rRNA*

To explore the underlying mechanism involved in *SNORD88C*/SCD1 axis, we first detected the effect of *SNORD88C* on SREBP1, an important transcription factor that regulates the expression of *SCD1* [16]. Unexpectedly, *SNORD88C* exerted no obvious effect on SREBP1 expression (Fig. 6A), indicating *SNORD88C* did not regulate transcription of *SCD1*, which was also confirmed by another observation that *SNORD88C* did not affect *SCD1* mRNA level (Fig. 6B). Thereby, we speculated that *SNORD88C* regulated SCD1 expression at the post-transcriptional level. Next, the proteasome inhibitor MG132 was used to block proteasomal degradation. However, MG132 treatment clearly increased SCD1 protein levels, but failed to reverse the regulation of *SNORD88C* on SCD1 (Fig. 6C), suggesting a protein-degradation-independent manner involved.

Previous studies have demonstrated box C/D snoRNAs are essential players in the rRNA biogenesis due to their involvement in guidance of 2′-O-me in the nucleolus, in turn regulation of protein translation in the cytoplasm [6]. Firstly, we performed fluorescence in situ hybridization (FISH) to detect the cellular distribution using Cy3-labeled probes targeting *SNORD88C*. As shown in Figs. 6D, S7A, *SNORD88C* was mainly located in the nucleolus and cytoplasm. This result was further validated by q-PCR in cytoplasmic/nuclear fractionation (Figs. 6E, S7B), indicating the potential of *SNORD88C* to directly regulate rRNA biological properties.

Moreover, we predicted *SNORD88C*-targeted rRNA through the snoPY database (http://snoopy.med.miyazaki-u.ac.jp/) based on bioinformatics, and found only *28S rRNA* contained a high complementary sequence to *SNORD88C*, and more important a potential site of c3680 for its-guided 2′-O-me (Fig. 6F). Then, primers that could distinguish the precursor (*ITS-28S*) and total *28S rRNA* were used to quantify, nevertheless, no significant changes

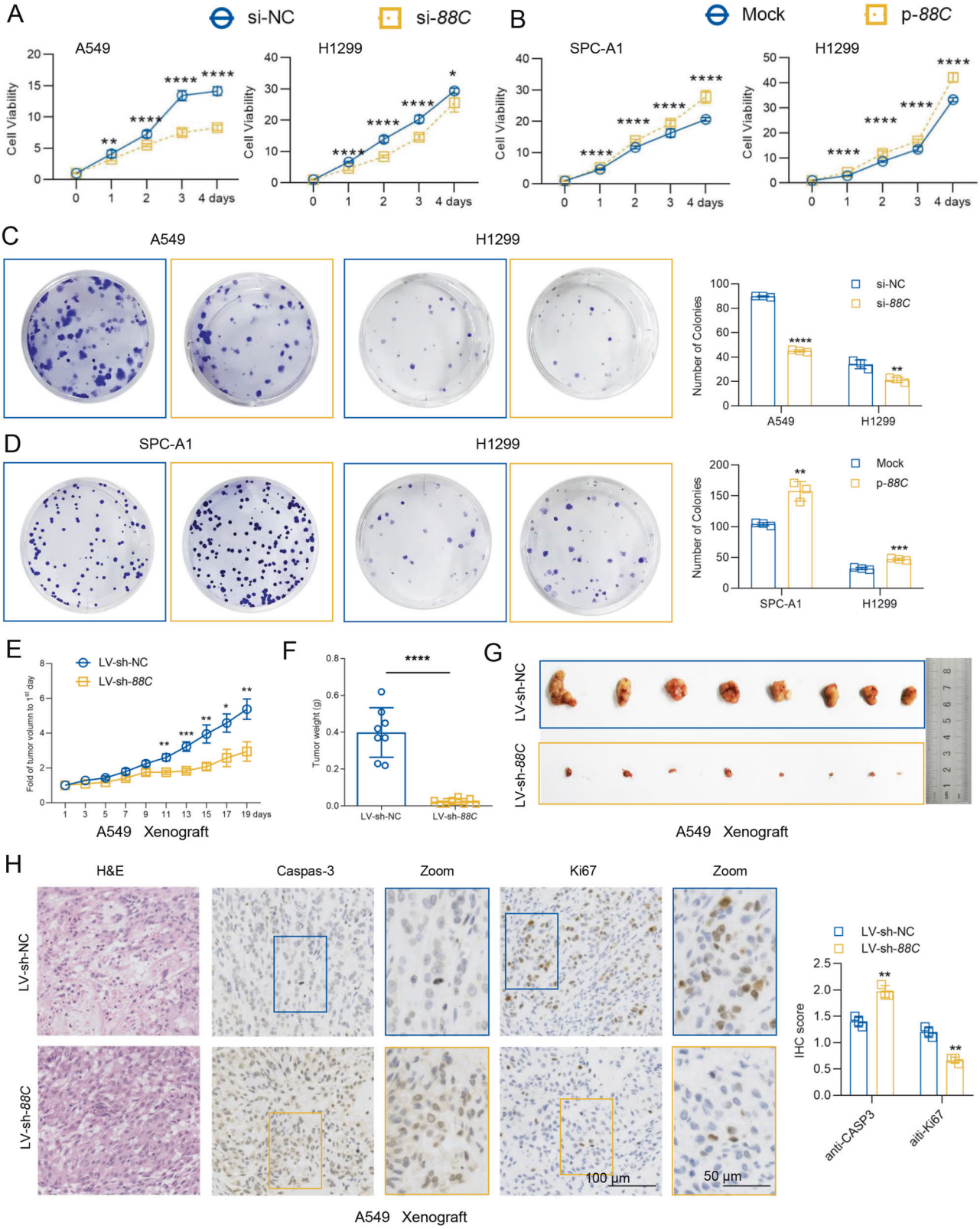

Fig. 2 *SNORD88C* promotes proliferation of NSCLC in vitro and in vivo. CCK8 (**A**, **B**) and clone formation (**C**, **D**) assays showed that knockdown of *SNORD88C* inhibited proliferation (**A**) and clonogenicity (**C**) in A549 and H1299 cells, while overexpression of *SNORD88C* in SPC-A1 and H1299 cells showed the opposite effect (**B**, **D**). In the A549 tumor transplantation model, the growth rate (**E**) of xenograft was slower, and the weight (**F**) and volume (**G**) decreased in LV-sh-*SNORD88C* compared with the control. **H** Immunohistochemical staining showed that the expression of Caspas-3 increased and the expression of Ki67 decreased in the tumor tissue of LV-sh-*SNORD88C* group compared with the control. Scale bar indicates 50 μm and 100 μm.; Two-tailed unpaired *t*-test, Mann-Whitney test, one-way analysis of variance (ANOVA) or Kruskal-Wallis test; **P* < 0.05, ***P* < 0.01, ****P* < 0.001, *****P* < 0.0001.

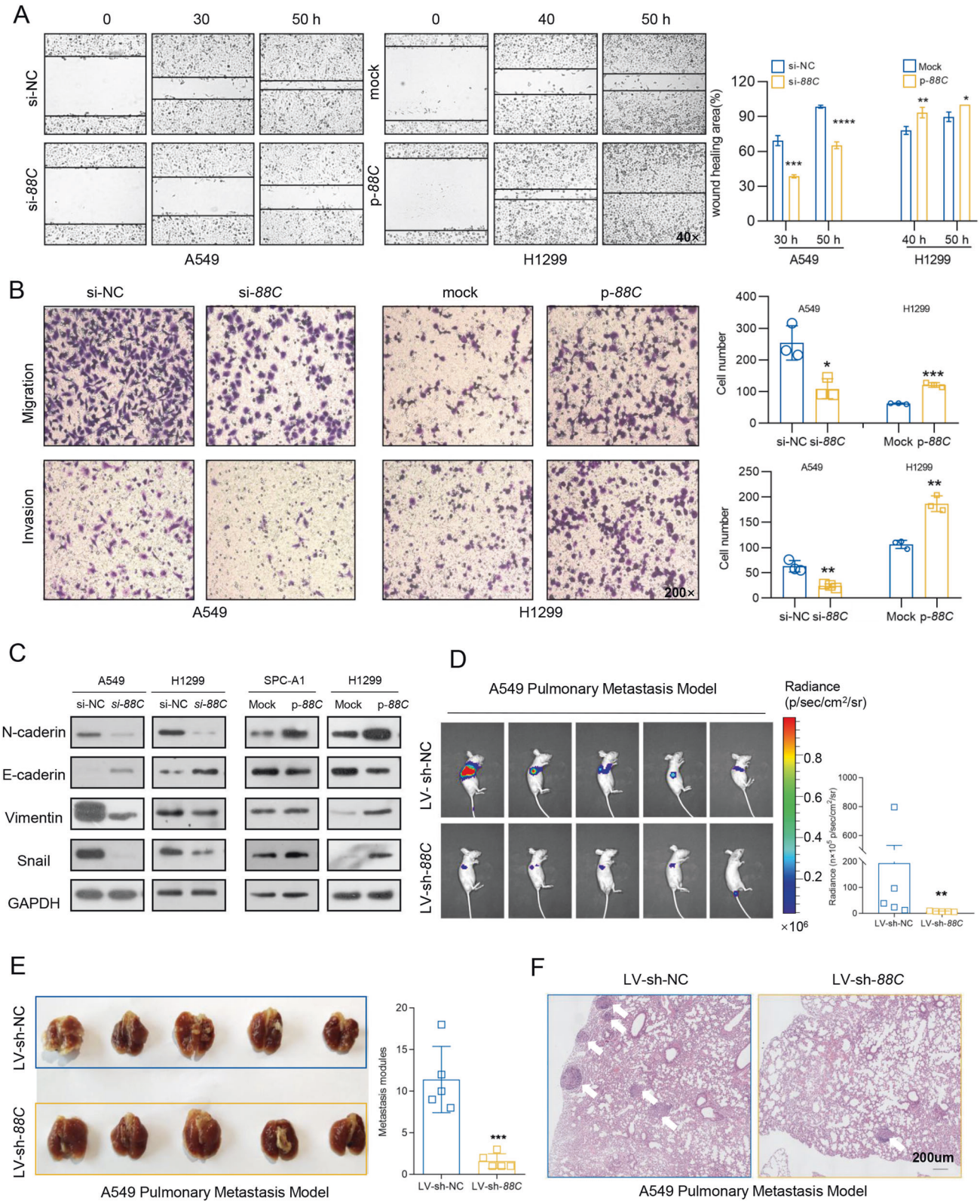

Fig. 3 ***SNORD88C* promotes NSCLC migration and invasion in vitro and in vivo. A**, **B** Wound healing, migration and invasion assays showed that knockdown of *SNORD88C* in A549 cells inhibited the motility, migration and invasion of NSCLC, while overexpression of *SNORD88C* in H1299 cells showed the opposite effect. Original magnification for wound healing, ×40; Original magnification for migration and invasion, ×200. **C** Western blot showed that *SNORD88C* knockdown decreased the expression of N-cadherin, Vimentin, and Snail and increased E-cadherin expression in A549 and H1299, while overexpression of *SNORD88C* showed the opposite expression for these proteins in SPC-A1 and H1299 cells. **D**, **E** In A549 pulmonary metastasis model the luciferase signal intensities in the LV-sh-*SNORD88C* group was remarkably lower than that in the control. **F** H&E staining showed that metastatic nodules in the lung tissue invaded the pulmonary capsule in the LV-sh-NC group, but not in the LV-sh-*SNORD88C*. Scale bar indicates 200 μm; Two-tailed unpaired *t*-test, $^{*}P < 0.05$, $^{**}P < 0.01$, $^{***}P < 0.001$, $^{****}P < 0.0001$.

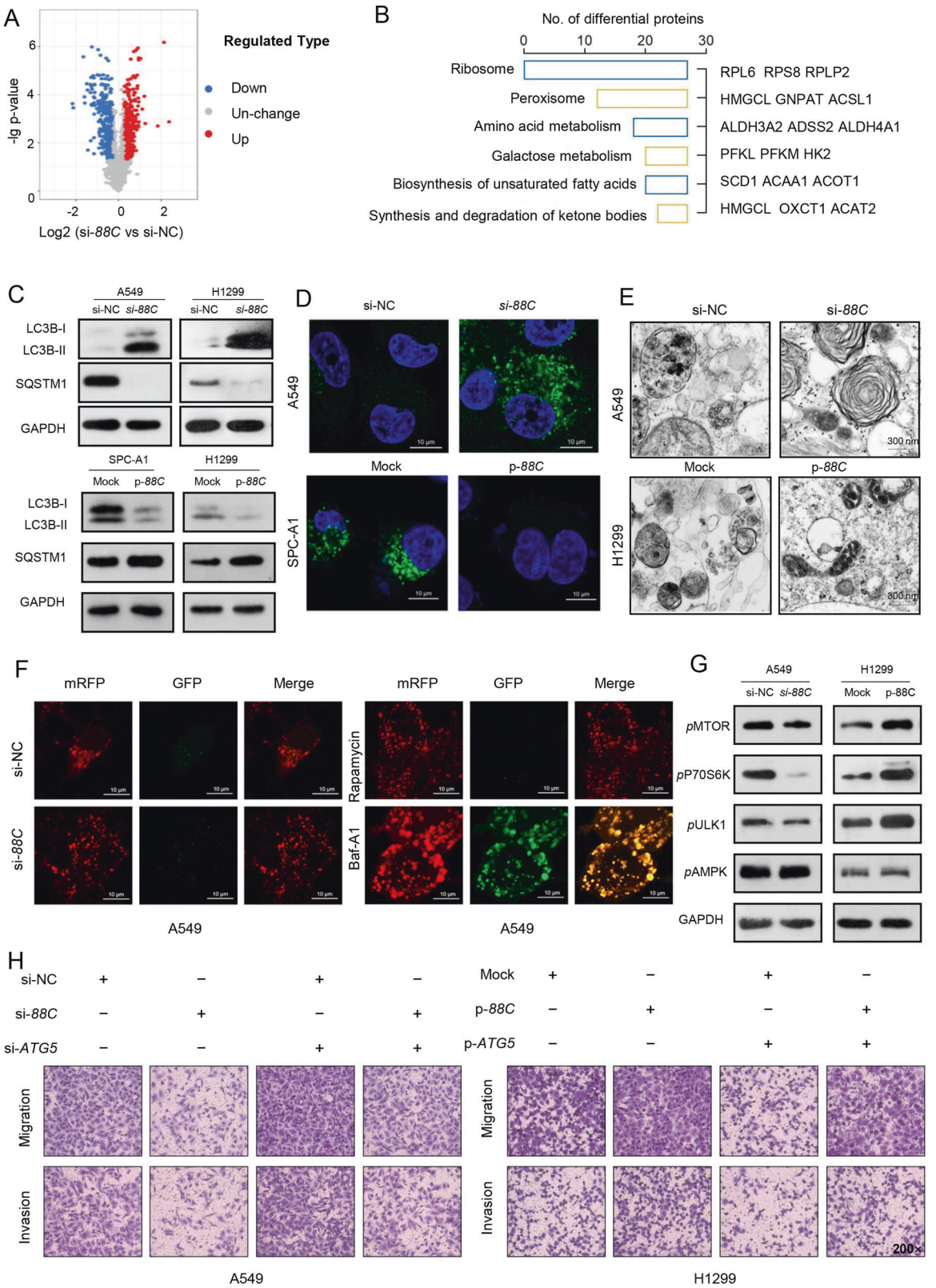

of mature *28S rRNA* were observed neither in *SNORD88C*-knockdown A549 cells nor in *SNORD88C*-overexpression H1299 cells (Table S4, Fig. 6G). Next, RTL-P assay, an approach based on reverse transcription with limiting dNTP concentration (Table S5), was used to confirm *SNORD88C*-guided 2′-O-me of *28S rRNA*. *SNORD88C* knockdown dramatically reduced the 2′-O-me of *28S rRNA* at the C3680 site under the lower dNTPs concentrations but not under the higher dNTPs in A549 cells (Fig. 6H). Meanwhile, overexpression of *SNORD88C* elevated the 2′-O-me activity under the lower dNTPs concentrations (Fig. 6I). Previous studies had demonstrated 2′-O-me would lead to the enhancement of rRNA-induced translational accuracy, and then prolong protein half-life

Fig. 4 *SNORD88C*-attenuated autophagy is required for its promotion of migration and invasion. A The volcano map showed that the differential proteins analyzed by LC-MS/MS-based TMT-labeled quantitative proteomic in *SNORD88C*-knockdown H1299 cells and the control group. ($p \leq 0.05$ and FC ≥ 1.2) **B** The differential proteins enrichment pathways. **C**–**E** WB, immunofluorescence labeled by anti-LC3 antibody as well as transmission electron microscopy showed that autophagy was activated in *SNORD88C*-knockdown NSCLC cells, but inhibited in *SNORD88C*-overexpression NSCLC cells. Scale bar indicates 10 μm and 300 μm. **F** A549 cells expressing mRFP-GFP-LC3 were transfected with si-NC or si-*88C*, or treated with 1 nM rapamycin or 1 nM Baf-A1 for 24 h and imaged by confocal microscopy. Scale bars: 10 μm. **G** WB assay showed that the phosphorylation levels of MTOR, P70S6K, and ULK1 were decreased in *SNORD88C*-knockdown A549 cells, while the phosphorylation levels of these proteins were enhanced in *SNORD88C*-overexpression H1299 cells. The AMPK phosphorylation level was not affected by *SNORD88C* knockdown or overexpression. **H** *ATG5* silencing could reverse the inhibitory effect of *SNORD88C* knockdown on the migration and invasion of A549 cells (left). *ATG5* overexpression could abolish the promotion of *SNORD88C* overexpression on the migration and invasion of H1299 cells (right). Original magnification, ×200. Two-tailed unpaired *t*-test, $^{**}P < 0.01$.

[6, 17–20]. Thereby, in vitro translation assay was performed via addition of cycloheximide (CHX), an inhibitor of protein translation to block overall protein synthesis. As a consequence, the half-life of SCD1 protein was shortened in *SNORD88C*-knockdown A549 cells (Fig. 6J) but extended in *SNORD88C*-overexpression H1299 cells (Fig. 6K) when treated with CHX. Finally, to figure out the possibility *SNORD88C* affected translation directly, polysome profiling was analyzed. Ribosomes fractions in the cell lysate were divided into ribosomal subunits (40S and 60S), monosomes (80S) and polysomes. As shown in Fig. 6L, M, *SNORD88C* silencing or overexpression did not affect the distribution profile of ribosomes fraction (left), indicating that *SNORD88C* did not influence global translation. Nevertheless, *SNORD88C* silencing significantly decreased *SCD1* mRNA enrichment in the monosomes and polysomes fractions, altering its distribution from the heavier to the lighter ribosome fractions, whereas *SNORD88C* overexpression demonstrated the opposite effect (right), more directly proving that *SNORD88C* regulated the expression of SCD1 by affecting translation level.

DISCUSSION

A myriad of studies emerged associating snoRNA dysregulation with cancer progression [21]. In present study, we identified the crucial role of *SNORD88C* in NSCLC, *SNORD88C* was up-regulated in tissue and plasma and served as a non-invasive diagnostic biomarker for NSCLC. Besides, through loss of function and functional acquisition analysis, we confirmed that *SNORD88C* promoted the proliferation and invasion, and metastasis of NSCLC in vivo and in vitro. More importantly, *SNORD88C*-mediate 2′-O-me of *28S rRNA* was essential for the initiation and maintenance of cancer.

2′-O-me of rRNA is the most common chemical modification of SNORDs and the supplement to the mechanism in tumorigenesis such as in colorectal cancer, leukemia and liver cancer [8, 9, 22], but rarely in NSCLC. In current study, we demonstrated that *SNORD88C* regulated the translation of SCD1 activity though guiding 2′-O-me of *28S rRNA*. To illuminate this issue, we first confirmed *SNORD88C* was capable to increase SCD1 expression but not at the transcriptional level, because *SNORD88C* had no impact on the expression of *SCD1* mRNA and its upstream transcription factor SREBP1; Moreover, the proteasome inhibitor MG132 treatment failed to reverse the regulation of *SNORD88C* on SCD1, suggesting a protein-degradation independent manner involved. Direct evidence was obtained from RTL-P assay. Only *28S rRNA* contained a high complementary sequence to *SNORD88C* with a potential site of C3680 for its-guided 2′-O-me, through which *SNORD88C* dramatically elevated the 2′-O-me activity of *28S rRNA* under the lower dNTPs concentrations but not under the higher dNTPs concentration. Translation inhibition experiments also proved that the half-life of SCD1 protein was prolonged by *SNORD88C* after the addition of CHX. In addition, polysome profiling assay more fully confirmed that *SNORD88C* regulated the expression of SCD1 protein by altering the distribution of *SCD1* mRNA in ribosomal fractions without affecting global translation. These results support that *SNORD88C* affect the translation fidelity of SCD1 through regulating 2′-O-me activity of *28S rRNA* at C3680.

SCD1, a rate-limiting enzyme responsible for MUFA synthesis, catalyzes the desaturation of saturated fatty acids [23]. Indeed, we proved *SNORD88C* induced abnormal lipid peroxidation dependent on SCD1 expression, because the inhibitory effect of *SNORD88C* on lipid peroxidation could be successfully reversed by *SCD1*. In previous studies, many snoRNAs regulated lipid metabolism in a 2′-O-Me -independent manner. For example, *U32A*, *U33*, *U34*, and *U35A* participated in lipid metabolism at the post-transcriptional level in the cytoplasm by binding to target RNA [24]. Herein, we proved that *SNORD88C* regulated abnormal lipid metabolism dependent on it guided the 2′-O-me of *28S rRNA*.

Accumulating evidence have proved the connection between SCD1 and the autophagic process based on it regulated lipid abnormalities [25]. Autophagy, a catabolic process that provides cells with tremendous metabolic plasticity and a major reactive survival mechanisms by protecting cells from stress factors such as nutritional deprivation [26], is regulated by various metabolic imbalances [27]. However, the controversial role of SCD1-mediated autophagy was observed in cancer. For example, SCD1 inhibition led to a mild autophagy reduction in cervical cancer HeLa cells [28], but an opposite trend was reported in the colon cancer cell line HCT-116 [29]. In current study, we demonstrated *SNORD88C* increased SCD1 translation, in turn, exerted inhibitory role in autophagy. This was because SCD1 maintained mTOR activity through modulation of MUFA availability, which prevented overactivation of autophagy, consistent with the previous study [30]. Nevertheless, autophagy is implicated in both metastasis-suppressive and -promoting biological activities in cancer [31]. For example, autophagy promoted liver cancer cell invasion by activating TGF-β/Smad3 signaling under starvation [32] but suppressed breast cancer metastasis by degrading NBR1 [33]. Our results confirmed that *SNORD88C*/SCD1 inhibited autophagy, then promoted lung cancer metastasis, consistent with the previous studies autophagy inhibition in multiple mammary cancer models accelerates the proliferation of disseminated tumor cells (DTCs) into overt macro-metastases [31]. One plausible explanation is that autophagy is required to maintain tumor cells in a dormant state and cellular homeostasis [34, 35], thus restricted the different phenotypic transitions of tumor cell; another is that autophagy degraded metastasis-related molecules [36] or specific tissue type [37] led to the inhibition of metastasis by autophagy. However, the more precise reasons need to be further studied to discuss.

Taken together, we found that *SNORD88C* was a new oncogenic snoRNA in NSCLC. We proved *SNORD88C* was up-regulated in tissue and plasma and served as a non-invasive diagnostic biomarker; then confirmed that it promoted proliferation and metastasis of NSCLC in vitro and in vivo. Importantly, *SNORD88C* guided *28S rRNA* methylation, which significantly increased the translation activity of downstream target gene *SCD1*. As a rate-limiting enzyme responsible for MUFA synthesis, SCD1 inhibited autophagy to further promote metastasis, providing the novel insight into the regulation of *SNORD88C* in NSCLC.

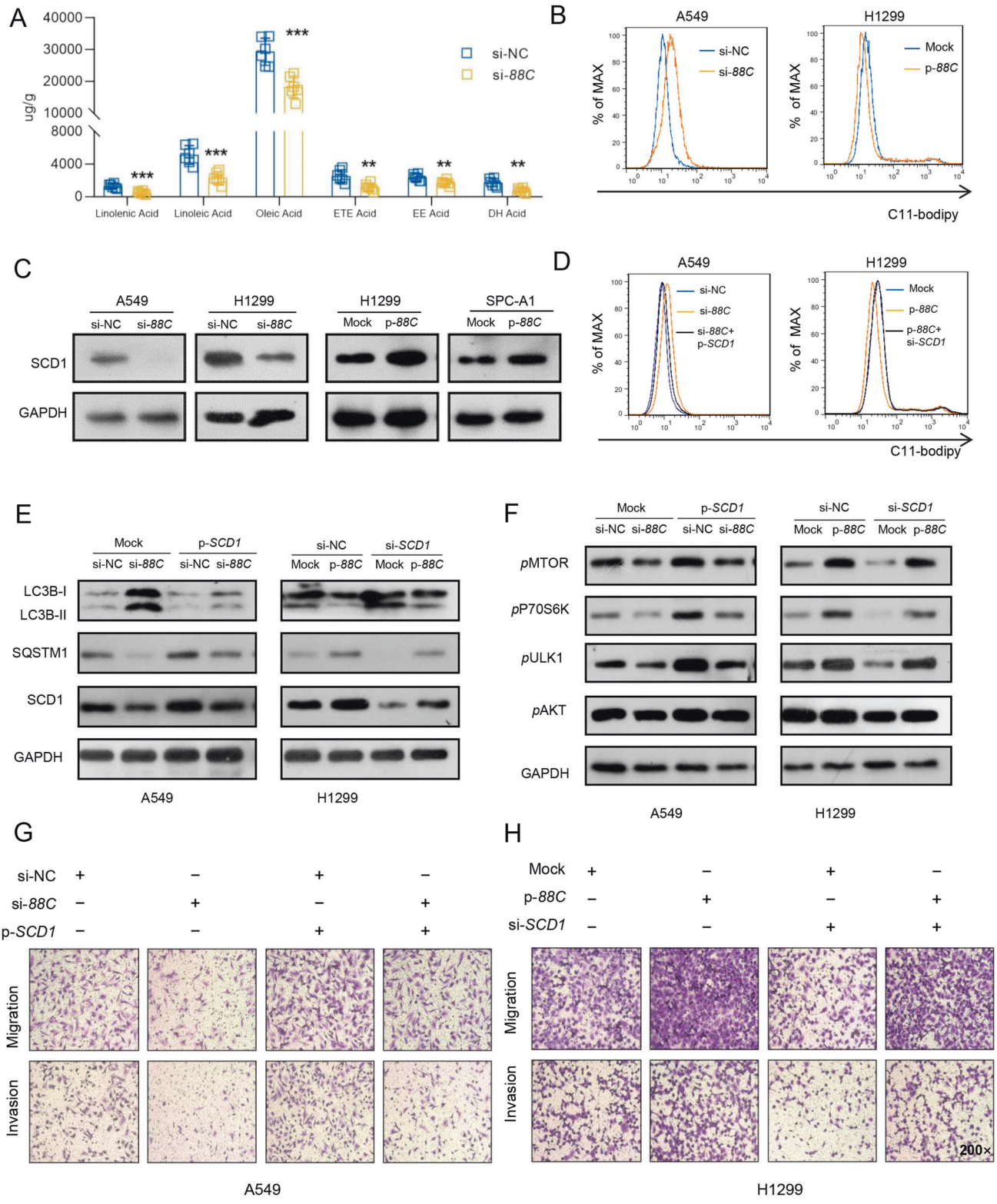

MATERIALS AND METHODS

Patients and Healthy donors

A total of 989 NSCLC cases with available clinical information and 91 matched normal lung tissues were included in the LUAD ($n = 513$) and LUSC ($n = 476$) cohorts of The Cancer Genome Atlas (TCGA). The snoRNAs gene expression data set of the above samples was downloaded from the SNORic database (http://bioinfo.life.hust.edu.cn/SNORic). FFPE samples of NSCLC and paired para-cancerous tissue from total 48 NSCLC patients and plasma samples from a total of 178 healthy volunteers and 224 NSCLC patients were collected from Shandong Cancer Hospital between September 2018 and July 2019. All patients didn't receive any anti-tumor treatment before samples collection, or suffer any other endocrine, immune, or metabolic diseases. The healthy donors did not present any disease. Detailed clinicopathological information was provided in Tables 1, 2, S1. The diagnosis of cancer was confirmed by two pathologists. Tumor stage was determined

Fig. 5 *SNORD88C* inhibits autophagy via upregulating SCD1 protein expression. A GC-MS-based metabolomics targeting fatty acids showed many kinds of unsaturated fatty acids were decreased in *SNORD88C*-knockdown H1299 cells compared to the control group. **B** Flow cytometry showed that through C11-bodipy staining, lipid peroxidation was promoted in *SNORD88C*-knockdown A549 cells, while inhibited in *SNORD88C*-overexpression H1299 cells. **C** WB showed that SCD1 expression was decreased in *SNORD88C*-knockdown A549 and H1299 cells, and increased in *SNORD88C*-overexpression SPC-A1 and H1299 cells. **D** The promotion of lipid peroxidation by *SNROD88C* knockdown in A549 cells and the inhibition of lipid peroxidation by *SNROD88C* overexpression in H1299 cells could be reversed by *SCD1* overexpression and knockdown. **E** In A549, the overexpression of *SCD1* reversed the increase of LC3B and the decrease of SQSTM1 caused by *SNORD88C* silencing. In H1299, knocking down *SCD1* abolished the decrease of LC3B and the increase of SQSTM1 induced by *SNORD88C* overexpression. **F** *SCD1* overexpression reversed the decreased phosphorylation of MTOR, P70S6K, and ULK1 caused by *SNORD88C* knockdown in A549. *SCD1* knockdown abolished the increased phosphorylation of these proteins induced by *SNORD88C* overexpression in H1299. **G** In A549, *SCD1* overexpression could reverse the inhibitory effect of *SNORD88C* knockdown on migration and invasion. **H** In H1299, *SCD1*-knockdown could abolish the promoting effect of *SNORD88C* overexpression on the migration and invasion. Original magnification, ×200. Two-tailed unpaired *t*-test, $^{**}P < 0.01$, $^{***}P < 0.001$.

according to the 8th edition of the lung cancer TNM staging standards formulated by IASLC.

SnoRNA-sequencing

The snoRNA-sequencing and data analysis were conducted by Aksomics (Shanghai, China). Total RNAs were extracted from 10 plasma samples (4 healthy volunteers and 6 NSCLC patients, including 3 early-stage and 3 advanced-stage patients). Agarose electrophoresis was used to check the integrality of total RNA samples, and then the samples were quantified on the NanoDrop ND-1000 instrument. 1~2ug total RNA of each sample was taken for SnoRNAseq library preparation. The library was denatured with 0.1 M NaOH to generate single-stranded DNA molecules, and amplified in situ using NovaSeq 6000 S4 Reagent Kit. Sequencing was carried out by running 150 cycles on Illumina NovaSeq 6000 according to the manufacturer's instructions. Sequencing quality was examined by FastQC software and trimmed reads were aligned to the Ensemble using NovoAlign software (v2.07.11). The expression profiling and differential expression of snoRNAs were calculated based on normalized TPM [38]. Hierarchical clustering, scatter plots and classification analysis were performed with the differential snoRNAs in R or Perl environment for statistical computing and graphics. Differential snoRNAs with statistical significance between the two groups were identified through *p*-value ≤ 0.05.

Cell culture

Human NSCLC cells A549, SPC-A1 and H1299 were purchased from the Cell Bank of the Chinese Academy of Sciences (Shanghai, China) or American Type Culture Collection (Manassas, VA, USA), and cultured in DMEM medium (Gibco, Carlsbad, CA, USA) containing 10% fetal bovine serum (FBS; Gibco) and antibiotics (penicillin/streptomycin, 100 U/ml) at 37 °C, 5% CO_2. Mycoplasma PCR testing of these cells was performed every month.

Transfection and siRNA interference

Human full-length *SNORD88C* cDNA (NR_003069.1) was synthesized by Genewiz (Suzhou, China) and cloned into the pCDH-CMV-MCS-EF1α-Puro vector (SBI, CD510B), named as p-*SNORD88C*; *SCD1* cDNA and *ATG5* cDNA were both synthesized by GenePharma (Shanghai, China) and respectively cloned into the pcDNA3.1(+) vector and p-ENTER vector, named as p-*SCD1* and p-*ATG5*. siRNAs of *SNORD88C*, *ATG5*, and *SCD1*, as well as the negative control RNA (si-NC) were purchased from Genepharma (Shanghai, China), sequences of siRNAs were listed in Table S3. Transfection of expressive vectors and siRNA interference were performed using Lipofectamine 3000 according to the manufacturer's protocols (Invitrogen).

For stable *SNORD88C* KD, lentiviruses expressing shRNA hairpins targeting human *SNORD88C* and firefly luciferase was designed and produced based on reporter vector CV344 by Genechem Company (Shanghai, China), named LV-sh-*SNORD88C*. A549 cells were transfected with 5 μl lentivirus with titer of 2×10^8 Tu/ml lentiviral plasmid containing or not containing the target gene. The medium containing 5 μg/ml puromycin was used for screening after co-culture for 48 h. The medium was replaced once 1-2 d to continue pressurized screening for a total of 10 d.

RNA extraction, reverse transcription and q-PCR

Total RNAs of cells and plasma were isolated by adding Trizol and Trizol LS, respectively (Thermo Fisher Scientific, MA, USA) according to manufacturer's instructions. In some experiments, nucleus, and cytoplasm needed to be separated first using Nuclear & Cytoplasmic RNA purification kit (NORGEN, Ontario, Canada). Total RNAs of FFPE samples were extracted using miRNAprep Pure FFPE kit (Tiangen Biotech, Beijing, China).

The extracted RNA was reverse transcribed to cDNA using Mir-X™ miRNA First-Strand Synthesis Kit and PrimeScript™ II 1st Strand cDNA Synthesis Kit (TaKaRa Bio, Nojihigashi, Kusatsu, Japan). qPCR was performed using TB-Green Premix Ex Taq II Reagent (TaKaRa Bio) and the primers for genes were presented in Table S2. Transfection efficiency was assessed using the $2^{-\Delta\Delta Ct}$ method and relative quantification was analyzed using ΔCt ($\Delta Ct = Ct^{snoRNA} - Ct^{U6}$) method. *U6* was used as the endogenous control of *SNORD88C*, while actin as the control of *SCD1*, *ATG5* and *C19orf48*.

In vitro proliferation, colony formation, wound-healing, migration and invasion assays

For cell proliferation assay, twenty-four hours following transfection, 1000–3000 transfected NSCLC cells were incubated in 96-well-plate for indicated time points and OD value was measured at 450 nm using Cell Counting Kit-8 every 24 h according to the manufacturer's instructions. Cell viability was calculated according to the formula: experimental OD value/control OD value × 100%

For colony formation assay, 100–200 transfected NSCLC cells were plated on a 6-well plate for 2 weeks. Cell colonies were fixed with 4% fixative solution (Solarbio, Beijing, China) and stained with gentian violet solution at room temperature for 30 min. colonies that consisted of >50 cells were counted and calculated. The colony formation efficiency was calculated with the following formula: Survival Fraction = Clones/Cell numbers × 100%.

For wound-healing assay, the transfected NSCLC cells were grown to a single layer covering the ground in six-well plate. A sterile 200 μl pipette tip was used to scrape the cell surface to create artificial wounds. The wound healing area was recorded under the microscope (Olympus, Japan) at three time points and analyzed using Fiji ImageJ software.

For migration assay, 5×10^4 transfected NSCLC cells were seeded in the upper chamber of transwell inserts (Corning, NY, USA) containing a polycarbonate membrane with 8.0 μm pores under serum-free conditions. The lower chamber was filled with 700 μl normal medium. After incubation for indicated time, cells on the upper surface of the membrane were completely removed by wiping with a cotton swab and fixed with 4% paraformaldehyde and stained with gentian violet for 30 min, then counted under the microscope (Olympus, Japan). For invasion assay, the transwell inserts were coated with Matrigel matrix (BD Science, USA).

Western blots

NSCLC cells were lysed in Cell Lysis Buffer (Beyotime, Beijing, China) supplemented with 0.5 mM PMSF (Beyotime), and the total cellular protein concentration was determined with a BCA Protein Assay Kit (Thermofisher). 50 μg protein was separated on SDS-PAGE and transferred onto PVDF membranes (Millipore, Billerica, MA, USA). Membranes were then blocked in TBST containing 5% evaporated skimmed milk (Bio-rad, USA) for 2–4 h, and then incubated overnight at 4 °C with the following primary antibodies: antibodies against human E-cadherin (14472), N-cadherin (13116), Vimentin (5741), LC3B (3868), SQSTM1 (88588), *p*AKT (4060), *p*AMPK (50081), *p*MTOR (5536), *p*P70S6K (9234). *p*ULK1 (14202), Snail (3879), SCD1 (2794) (all 1:1000; Cell Signaling Technology, CST, Massachusetts, USA), GAPDH (10494–1-AP) (1:1000, Proteintech Group), SREBP1 (sc-13551) (1:100, Santa Cruz Biotechnology), followed by incubation with horseradish peroxidase coupled secondary anti-mouse (7076) or anti-

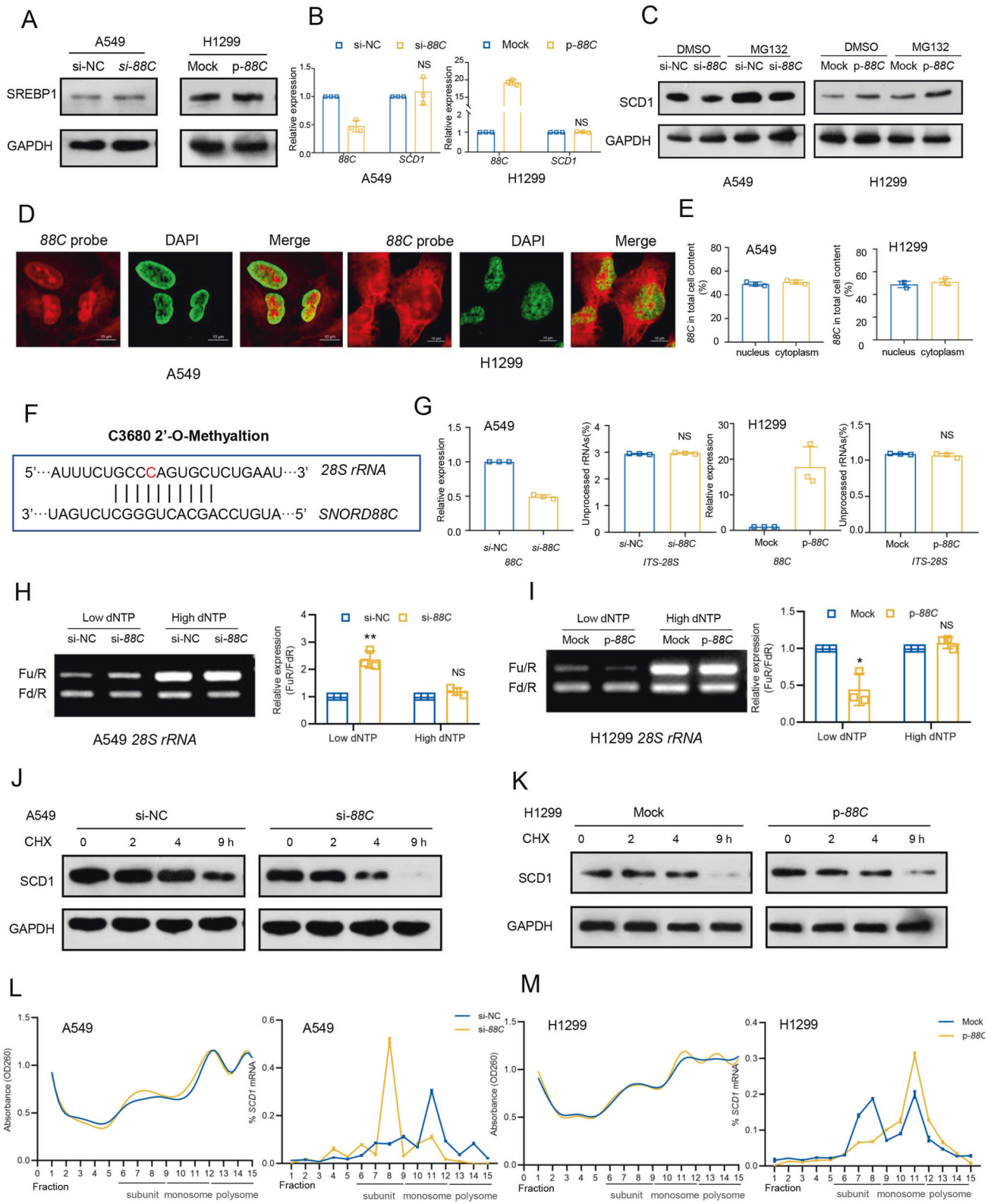

rabbit antibodies (7074) (1:2000; CST) for 1 h at room temperature. The protein bands were visualized using ECL blotting detection reagents (Bio-Rad, USA), and then developed and fixed onto x-ray films. GAPDH was served as a loading control. In some experiments, 50 μg/mL CHX was added to the culture medium, followed by incubation for 0 h, 2 h, 4 h, or 9 h.

A549 tumor xenografts model and pulmonary metastasis model

For tumor xenografts model, sixteen 6-week-old male BALB/c-nude mice purchased from Beijing HFK Bioscience Co. Ltd. (Beijing, China) were randomly divided into two groups, a total of 5×10^6 A549 cells with LV-sh-NC or LV-sh-*SNORD88C* were respectively injected subcutaneously into the

Fig. 6 *SNORD88C* regulates the translation activity of SCD1 though guiding 2′-O-me of *28S rRNA*. **A** Western blot showed that SREBP1 expression was not affected by *SNORD88C* knockdown or overexpression. **B** q-PCR showed that *SCD1* mRNA level was not affected by *SNORD88C* knockdown or overexpression. **C** Western blot showed MG132 treatment clearly increased SCD1 protein levels, but failed to reverse the regulation of *SNORD88C* knockdown or overexpression on SCD1. **D**, **E** Fluorescent in situ hybridization (FISH) using Cy3-labeled probes targeting *SNORD88C* and q-PCR showed *SNORD88C* was mainly located in the nucleolus and cytoplasm. Red represented *SNORD88C*, green (artifact) represented nucleus. Scale bar indicates 10 μm. **F** The snoPY database predicted the complementary sequence and 2′-O-me site of rRNA targeted by *SNORD88C*, and red represented the methylation site. **G** q-PCR assay to detect *ITS-28S* showed that *SNORD88C* knockdown (left) or overexpression (right) did not affect the processing of *28S rRNA*. The value of the vertical coordinate represented the average of primer pairs d/c (unprocessed) over b/a (total) and primer pairs f/e (unprocessed) over b/a (total) for *28S rRNA*, respectively. Primers were shown in Table S4. **H**, **I** The 2′-O-me activity of *28S rRNA* at C3680 site detected by RTL-P assay was decreased after *SNORD88C* knockdown in A549, while increased after *SNORD88C* overexpression in H1299. **J**, **K** The translation activity of SCD1 was reduced by *SNORD88C* knockdown treated by the CHX in A549 cells, while increased by *SNORD88C* overexpression in H1299 cells. Two-tailed unpaired t test; ns, no significance; $^{*}P < 0.05$, $^{**}P < 0.01$. **L**, **M** Ribosomal components in cytoplasmic extracts of si-NC and si-*88C* A549 cells (**L**) or mock and p-*88C* H1299 cells (**M**) were fractionated through sucrose gradients, and the relative levels of *SCD1* mRNA were analyzed by qRT-PCR in the gradient fractions.

right flank region of each mouse. After visible tumors had developed, tumor volume was measured and calculated as (length × width^2)/2 every 2 days. Five weeks after injection, the mice were sacrificed, and the tumor nodules were harvested and weighed.

For pulmonary metastasis model, ten 6-week-old male BALB/c-nude mice purchased from Beijing HFK Bioscience Co. Ltd. (Beijing, China) were randomly divided into two groups and a total of 1×10^6 A549 cells with stable firefly luciferase expression and silenced *SNORD88C* (LV-sh-*SNORD88C*), as well as the negative control (LV-sh-NC) were injected to the tail vein. Bioluminescent NSCLC metastases were monitored weekly via the IVIS Spectrum In Vivo Imaging System (PerkinElmer, USA). One month after injection, the mice lungs were harvested, fixed, weighed and stained. These mice were purchased from HFK Bioscience (Beijing, China). The Institutional Animal Care and Use Committee of Shandong Cancer Hospital and Institute approved these experiment procedures.

Immunohistochemistry

The paraffin-embedded tissues were cut into 4-μm sections and then analyzed by immunohistochemistry (IHC) using antibodies against Ki67 and CASPAS 3. The staining intensity and corresponding percentage were evaluated independently by two pathologists to confirm the reproducibility of the results. The intensity of staining was scored on a 0–2 scale, with no staining = 0, weak staining = 1, and strong staining = 2. The staining score was calculated according to the formula: IHC score = P1 × 1 + P2 × 2 + P3 × 3 (P: percentage).

Immunofluorescence (IF) staining and fluorescent in situ hybridization (FISH)

For IF staining, NSCLC cells were fixed with 4% paraformaldehyde after adherent growth on the climbing slice and permeabilized with 0.1% Triton X-100 for 15 min. After incubation with primary antibody against human anti-LC3B (CST) for 1 h, cells were incubated with Alexa 488-conjugated (1:1000) (Abcam) secondary antibodies for 1 h. Nucleus was stained with DAPI for 3 min (Beyotime). Images were acquired on a confocal laser microscopy (LSM800, Carle Zeiss, Germany) For quantification of the number of autophagosomes (diameters 0.3–1.0 μM), at least three cells were randomly chosen, all eligible puncta were recorded and analyzed using Fiji ImageJ software.

For FISH, *SNORD88C*-specific Cy3 fluorescence-labeled probe (5′-3′: TGTGTCCTCAGGGGTGATCAGAGCC) and fluorescence in situ hybridization kit (Genepharma, Shanghai, China) were used in FISH experiment. Briefly, the cells were inoculated on small chamber slides, fixed with 4% paraformaldehyde, and then exposed to 0.5% TritonX-100. After denaturation at 73 °C for 5 min, the probe was added to the cell culture medium and hybridized and incubated overnight After full washing, the nucleus was stained with DAPI. The image was captured on confocal laser microscopy.

Transmission electron microscopy (TEM)

TEM samples preparation and observation were performed by Weiya biotech Co., Ltd (Jinan, PR China). The NSCLC cells were fixed in 4% glutaraldehyde solution at 4 C for 4 h and washed with 0.1 M phosphoric acid buffer (PH7.4) for 3 times, each time 15 min. After fixation in 1% osmium tetroxide for 2 h, the specimens were washed with 0.1 m phosphoric acid buffer again. After dehydrated through a graded series of ethanol, the samples were embedded in Epon (Sigma, 45347). Ultrathin sections were stained with 2% uranyl acetate and lead citrate, and observed using a transmission electron microscope (HT7700, Hitachi, Japan).

Adenoviral infection

Recombinant adenoviral vector carrying the human mRFP-GFP-LC3 gene was purchased from HanBio (Shanghai, China). Cells were plated in 12-well plates at a density of 1×10^4 cells per well and infected at an MOI of 2 with GFP-mRFP-LC3 gene for 24 h. After washing with PBS twice, cells were transfected with si-NC or si-*88C* or treated with rapamycin or Baf.A1 for another 24 h respectively.

LC-MS/MS-based proteomics and GC-MS-based fatty acids metabolomics

For LC-MS/MS-based proteomics, the cultured H1299 cells were divided into two groups and transfected with si-*SNORD88C* and si-NC respectively. The proteins of the two groups were extracted and identified by TMT labeling, high-performance liquid chromatography (HPLC), and quantitative proteomics based on mass spectrometry (MS). All the identified proteins were analyzed systematically by bioinformatics, and all differential proteins were analyzed by functional classification, functional enrichment, and cluster analysis based on functional enrichment. Extraction, detection, and analysis of proteins are performed by Jingjie PTM Biolab Co. Ltd (Hangzhou, PR China).

For GC-MS-based fatty acids metabolomics, H1299 cells were divided into two groups transfected with si-*SNORD88C* or si-NC, and 6 independent samples were needed for the corresponding biological repeats of each group. All samples were quantified by BCA and then the abundance of free fatty acids was detected on the GC/MS platform. Detection and analysis are performed by Shanghai Biotree biotech Co. Ltd. (Shanghai, PR China). The student's *t*-test ($p < 0.05$) was used to assess the significance of difference in abundance of free fatty acids between the two groups.

Measurement of lipid peroxidation

After, cells were stained with 5 μM C11-bodipy 581/591 lipid peroxidation fluorescent probe (ABclonal, RM02821) for 30 min, then digested with trypsin, re-suspended in PBS containing 5% FBS and analyzed by flow cytometry. The proportion of lipid peroxidation cells was quantified according to the arithmetic mean value ± SEM of histogram fluorescence signal.

RTL-P assay for rRNA 2′-O-methylation

2′-O-me of *28S rRNA* at C3680 site was measured as previously reported with minor modification [39]. The mixture containing specific RT primers, total RNA, and a low (10 μM) or high (1 mM) concentration of dNTPs was heated at 65 °C for 5 min and then was placed on ice, the specific primers were shown in Table S5. Next, 5 × PrimeScript II Buffer, RNase Inhibitor and PrimeScript II RTase were mixed into the reaction solution of the first step with an initial annealing step at 42 °C for 1 h and then mixture was heated at 95 °C for 5 min. The PCR reaction was determined using 2 × Taq Plus Master Mix II (Dye Plus) (Vazyme, Nanjing, China), and the agarose gel electrophoresis was carried out to detect rRNA methylation.

Table 1. Characteristics of NSCLC patients for *SNORD88C* in FFPE specimens.

Parameters	Samples, *n*	*SNORD88C* expression	
		Δ Ct Median (interquartile range)	*P*-value
Age (years)			
≤62	24	5.378 (4.240–5.873)	0.0609
>62	24	4.695 (3.951–5.038)	
Gender			
Male	32	4.855 (3.994–5.561)	0.5053
Female	16	4.885 (4.396–5.921)	
Smoking			
NO	18	5.065 (4.240–5.814)	0.5316
YES	27	4.915 (3.945–5.580)	
Not Available	3		
Drinking			
N0	23	5.115 (4.210–5.975)	0.3300
YES	21	4.915 (3.958–5.463)	
Not Available	4		
Histology			
AC	24	5.065 (4.049–5.953)	0.5362
SCC	24	4.775 (4.101–5.484)	
Tumor size			
V > 6 cm^3	22	5.080 (4.200–5.689)	0.9955
V ≤ 6 cm^3	23	4.710 (3.970–5.760)	
Not available	3		
T stage			
T1	26	5.065 (4.150–5.848)	0.3108
T2	14	4.525 (2.880–5.401)	
T3	3	5.300 (4.915–5.505)	
T4	2	5.595 (5.045–6.145)	
TX	3		
LN meta.			
N0	32	5.080 (4.066–5.734)	0.3334
N1	4	5.265 (4.331–6.000)	
N2	4	3.803 (-0.7300–5.046)	
N3	4	5.015 (2.344–6.651)	
NX	4		
Distant meta.			
M0	44	5.030 (4.229–5.734)	
M1	1	1.560	
MX	3		
TNM stage			
I	25	5.115 (3.958–5.823)	
II	9	4.915 (4.283–5.670)	
III	9	5.045 (3.803–5.740)	
IV	1	1.560	
Not available	4		

Table 2. Characteristics of NSCLC patients for *SNORD88C* in plasma.

Parameters	Samples, *n*	*SNORD88C* expression	
		Δ Ct Median (interquartile range)	*P*-value
Age (years)			
<62	105	6.050 (5.280–6.455)	0.7496
≥62	119	5.990 (5.200–6.570)	
Gender			
Male	134	6.080 (5.165–6.630)	0.5101
Female	90	5.990 (5.368–6.368)	
Smoking			
No	111	6.070 (5.440–6.460)	0.6028
Yes	111	5.910 (5.090–6.670)	
Not available	2		
Drinking			
No	168	6.110 (5.400–6.485)	0.3914
Yes	56	5.865 (4.970–6.685)	
Histology			
AC	158	6.005 (5.285–6.443)	0.4673
SCC	47	5.880 (5.200–6.690)	
Others	19		
Tumor size			
≤6 cm^3	80	6.105 (5.560–6.565)	**0.0490**
>6 cm^3	80	5.905 (5.083–6.438)	
Not available	64		
T stage			
Tis	8	6.175 (5.568–6.782)	**0.0142**
T1	68	6.124 (5.928–6.321)	
T2	70	5.877 (5.651–6.102)	
T3	17	5.625 (5.055–6.194)	
T4	42	5.569 (5.305–5.832)	
TX	19		
LN meta.			
N0	97	6.230 (5.665–6.615)	**0.0008**
N1	17	6.290 (5.570–6.695)	
N2	53	5.800 (5.060–6.360)	
N3	40	5.420 (4.873–6.285)	
NX	17		
Distant meta.			
M0	131	6.160 (5.550–6.600)	**0.0023**
M1	91	5.790 (5.050–6.360)	
MX	2		
TNM stage			
0	7	6.160 (5.630–6.840)	**0.0100**
I	69	6.250 (5.750–6.685)	
II	15	6.110 (5.610–6.690)	
III	39	5.880 (5.090–6.420)	
IV	92	5.800 (5.055–6.368)	
Not available	2		

Bold values represent statistical significance $p < 0.05$.

Polysome profiling

5×10^7 NSCLC cells were exposed to cycloheximide (200 μg/ml) for 5 min, and then were sufficiently lysed in 1000 μl of cytoplasmic lysis buffer containing polysome buffer 878 μl (1000 μl = 3 M NaCl 50 μl, 1 M $MgCl_2$ 5 μl, 1 M Tris HCL Ph7.5 20 μl, RNase free H_2O 925 μl), 10% Triton X-100 100 μl, 100 mM DTT 10 μl, 1U/μl DNase I 10 μl, 50 mg/ml cycloheximide 2 μl. After centrifugation at 2000 *g* at 4 °C for 15 minutes, the supernatant was observed and supplemented with the lysis buffer to make the RNA concentration in the supernatant of different samples consistent. RNA concentration was detected by Nano Drop one (Thermo Fisher Scientific, MA, USA).

For fractionation, the same volume supernatants were loaded into 10%-45% sucrose gradients and separated by ultracentrifugation with a SW41Ti rotor (Beckman Coulter, Brea, CA, USA) at 4 °C and 230,000 *g* for 3 hours. The centrifuged solution was equally divided into 15 equal fractions from top to bottom and then the OD 260 value of each fraction was measured. Subsequently, total RNA was extracted from each fraction, then subjected to RT-qPCR for *SCD1* mRNA analysis. Relative distribution of mRNA in each fraction was normalized with the sum of all fractions.

Statistical analysis

All the analyses were completed by SPSS 21.0 software (IBM, Ehningen, Germany) and GraphPad Prism version 8.0 (San Diego, CA, USA), with $P < 0.05$ being considered statistically significant. The normality of the distribution was checked using the Kolmogorov–Smirnov test. If the data followed normal analysis, unpaired t-test would be used; if not, Mann-Whitney test would be used. Chi-square test was used for analyzing categorical variables. Multi-group analysis was tested by one-way analysis of variance (ANOVA) or Kruskal-Wallis test. In paired data, the normally distributed numeric variables were evaluated by paired t-test, whereas non-normally distributed variables were analyzed by Wilcoxon rank-test. Receiving operating characteristic (ROC) curve was used to evaluate diagnostic efficiency. The data was presented as the median with interquartile range.

DATA AVAILABILITY

All relevant data are available from the corresponding author upon reasonable request. In addtion, raw data from snoRNA sequencing and protein mass spectrometry were uploaded to the GAS-Human (HRA003325) and OMIX (OMIX002173) databases of CNCB-NGDC (China National Center for Bioinformation-National Genomics Data Center).

REFERENCES

1. Bray F, Ferlay J, Soerjomataram I, Siegel RL, Torre LA, Jemal A. Global cancer statistics 2018: GLOBOCAN estimates of incidence and mortality worldwide for 36 cancers in 185 countries. CA Cancer J Clin. 2018;68:394–424.
2. Herbst RS, Morgensztern D, Boshoff C. The biology and management of non-small cell lung cancer. Nature 2018;553:446–54.
3. Mannoor K, Liao J, Jiang F. Small nucleolar RNAs in cancer. Biochim Biophys Acta. 2012;1826:121–8.
4. Liang J, Wen J, Huang Z, Chen XP, Zhang BX, Chu L. Small nucleolar RNAs: Insight into their function in cancer. Front Oncol. 2019;9:587.
5. Williams GT, Farzaneh F. Are snoRNAs and snoRNA host genes new players in cancer? Nat Rev Cancer. 2012;12:84–8.
6. Erales J, Marchand V, Panthu B, Gillot S, Belin S, Ghayad SE, et al. Evidence for rRNA 2′-O-methylation plasticity: Control of intrinsic translational capabilities of human ribosomes. Proc Natl Acad Sci USA. 2017;114:12934–9.
7. Pelletier J, Thomas G, Volarevic S. Ribosome biogenesis in cancer: new players and therapeutic avenues. Nat Rev Cancer. 2018;18:51–63.
8. Wu H, Qin W, Lu S, Wang X, Zhang J, Sun T, et al. Long noncoding RNA ZFAS1 promoting small nucleolar RNA-mediated 2′-O-methylation via NOP58 recruitment in colorectal cancer. Mol Cancer. 2020;19:95.
9. Liu Z, Pang Y, Jia Y, Qin Q, Wang R, Li W, et al. SNORA23 inhibits HCC tumorigenesis by impairing the 2′-O-ribose methylation level of 28S rRNA. Cancer Biol Med. 2021;19:104–19.
10. Okugawa Y, Toiyama Y, Toden S, Mitoma H, Nagasaka T, Tanaka K, et al. Clinical significance of SNORA42 as an oncogene and a prognostic biomarker in colorectal cancer. Gut 2017;66:107–17.
11. Tian B, Liu J, Zhang N, Song Y, Xu Y, Xie M, et al. Oncogenic SNORD12B activates the AKT-mTOR-4EBP1 signaling in esophageal squamous cell carcinoma via nucleus partitioning of PP-1alpha. Oncogene 2021;40:3734–47.
12. Liao J, Yu L, Mei Y, Guarnera M, Shen J, Li R, et al. Small nucleolar RNA signatures as biomarkers for non-small-cell lung cancer. Mol Cancer. 2010;9:198.
13. Zhao Y, Yan Y, Ma R, Lv X, Zhang L, Wang J, et al. Expression signature of six-snoRNA serves as novel non-invasive biomarker for diagnosis and prognosis prediction of renal clear cell carcinoma. J Cell Mol Med. 2020;24:2215–28.
14. Shang X, Song X, Wang K, Yu M, Ding S, Dong X, et al. SNORD63 and SNORD96A as the non-invasive diagnostic biomarkers for clear cell renal cell carcinoma. Cancer Cell Int. 2021;21:56.
15. Klionsky DJ, Abdel-Aziz AK, Abdelfatah S, Abdellatif M, Abdoli A, Abel S, et al. Guidelines for the use and interpretation of assays for monitoring autophagy (4th edition)(1). Autophagy 2021;17:1–382.
16. Yi J, Zhu J, Wu J, Thompson CB, Jiang X. Oncogenic activation of PI3K-AKT-mTOR signaling suppresses ferroptosis via SREBP-mediated lipogenesis. Proc Natl Acad Sci USA. 2020;117:31189–97.
17. Martinez-Miguel VE, Lujan C, Espie-Caullet T, Martinez-Martinez D, Moore S, Backes C, et al. Increased fidelity of protein synthesis extends lifespan. Cell Metab. 2021;33:2288–300.e12.
18. Andrade JM, Dos Santos RF, Chelysheva I, Ignatova Z, Arraiano CM. The RNA-binding protein Hfq is important for ribosome biogenesis and affects translation fidelity. EMBO J. 2018;37:e97631.
19. Bustelo XR, Dosil M. Ribosome biogenesis and cancer: basic and translational challenges. Curr Opin Genet Dev. 2018;48:22–9.
20. Chaillou T. Ribosome specialization and its potential role in the control of protein translation and skeletal muscle size. J Appl Physiol (1985). 2019;127:599–607.
21. Thorenoor N, Slaby O. Small nucleolar RNAs functioning and potential roles in cancer. Tumour Biol. 2015;36:41–53.
22. Zhou F, Liu Y, Rohde C, Pauli C, Gerloff D, Kohn M, et al. AML1-ETO requires enhanced C/D box snoRNA/RNP formation to induce self-renewal and leukaemia. Nat Cell Biol. 2017;19:844–55.
23. Wang H, Klein MG, Zou H, Lane W, Snell G, Levin I, et al. Crystal structure of human stearoyl-coenzyme A desaturase in complex with substrate. Nat Struct Mol Biol. 2015;22:581–5.
24. Caputa G, Schaffer JE. RNA regulation of lipotoxicity and metabolic stress. Diabetes 2016;65:1816–23.
25. Ascenzi F, De Vitis C, Maugeri-Sacca M, Napoli C, Ciliberto G, Mancini R. SCD1, autophagy and cancer: implications for therapy. J Exp Clin Cancer Res. 2021;40:265.
26. Kimmelman AC, White E. Autophagy and tumor metabolism. Cell Metab. 2017;25:1037–43.
27. Boya P, Reggiori F, Codogno P. Emerging regulation and functions of autophagy. Nat Cell Biol. 2013;15:713–20.
28. Ogasawara Y, Itakura E, Kono N, Mizushima N, Arai H, Nara A, et al. Stearoyl-CoA desaturase 1 activity is required for autophagosome formation. J Biol Chem. 2014;289:23938–50.
29. Ono A, Sano O, Kazetani KI, Muraki T, Imamura K, Sumi H, et al. Feedback activation of AMPK-mediated autophagy acceleration is a key resistance mechanism against SCD1 inhibitor-induced cell growth inhibition. PLoS One. 2017;12:e0181243.
30. Zhou X, Zhu X, Li C, Li Y, Ye Z, Shapiro VS, et al. Stearoyl-CoA desaturase-mediated monounsaturated fatty acid availability supports humoral immunity. Cell Rep. 2021;34:108601.
31. Chen HT, Liu H, Mao MJ, Tan Y, Mo XQ, Meng XJ, et al. Crosstalk between autophagy and epithelial-mesenchymal transition and its application in cancer therapy. Mol Cancer. 2019;18:101.
32. Li J, Yang B, Zhou Q, Wu Y, Shang D, Guo Y, et al. Autophagy promotes hepatocellular carcinoma cell invasion through activation of epithelial-mesenchymal transition. Carcinogenesis 2013;34:1343–51.
33. Marsh T, Debnath J. Autophagy suppresses breast cancer metastasis by degrading NBR1. Autophagy 2020;16:1164–5.
34. Ferraresi A, Girone C, Esposito A, Vidoni C, Vallino L, Secomandi E, et al. How autophagy shapes the tumor microenvironment in ovarian cancer. Front Oncol. 2020;10:599915.
35. Garcia-Prat L, Munoz-Canoves P, Martinez-Vicente M. Monitoring autophagy in muscle stem cells. Methods Mol Biol. 2017;1556:255–80.
36. Lv Q, Wang W, Xue J, Hua F, Mu R, Lin H, et al. DEDD interacts with PI3KC3 to activate autophagy and attenuate epithelial-mesenchymal transition in human breast cancer. Cancer Res. 2012;72:3238–50.
37. Cheong H, Lu C, Lindsten T, Thompson CB. Therapeutic targets in cancer cell metabolism and autophagy. Nat Biotechnol. 2012;30:671–8.
38. Bullard JH, Purdom E, Hansen KD, Dudoit S. Evaluation of statistical methods for normalization and differential expression in mRNA-Seq experiments. BMC Bioinforma. 2010;11:94.
39. Dong ZW, Shao P, Diao LT, Zhou H, Yu CH, Qu LH. RTL-P: a sensitive approach for detecting sites of 2′-O-methylation in RNA molecules. Nucleic Acids Res. 2012;40:e157.

ACKNOWLEDGEMENTS

We thank Hualei Yu for technical assistance of polysome profiling experiment and Xiujie Cui for the animal care.

AUTHOR CONTRIBUTIONS

SX and SX designed and conceived the research content. Wang Kangyu performed sample collection, experiments, data analysis and wrote the manuscript. SX guided the experiments and reviewed the manuscript. WS carried out the Western blot assay. ZY extracted RNA of FFPE samples. SX, XL, and SX contributed reagents materials, instruments, analytic tools, and grant support. The author(s) read and approved the final manuscript.

FUNDING

This work was supported by the National Natural Science Foundation of China (81972014), the Shandong Provincial Natural Science Foundation (ZR2019MH004 and ZR2019LZL016) and Shandong Provincial Key Research and Development Program (Major Science & Technology Innovation Project) (2021SFGC0501).

ETHICS STATEMENT

The studies involving human participants (201806004) and animals (201911025) were reviewed and approved by Ethics Committee of Shandong Cancer Hospital and Institute.

COMPETING INTERESTS

The authors declare no competing interests.

ADDITIONAL INFORMATION

Supplementary information The online version contains supplementary material available at https://doi.org/10.1038/s41418-022-01087-9.

Correspondence and requests for materials should be addressed to Xingguo Song or Xianrang Song.